Chapter

Coherent Receiver for Turbo Coded Single-User Massive MIMO-OFDM with Retransmissions

K. Vasudevan, Shivani Singh and A. Phani Kumar Reddy

Abstract

Single-user massive multiple-input multiple-output (MIMO) systems have a large number of antennas at the transmitter and receiver. This results in a large overall throughput (bit-rate), of the order of tens of gigabits per second, which is the main objective of the recent fifth-generation (5G) wireless standard. It is feasible to have a large number of antennas in mm-wave frequencies, due to the small size of the antennas. This chapter deals with the coherent detection of orthogonal frequency division multiplexed (OFDM) signals transmitted through frequency-selective Rayleigh fading MIMO wireless channels. Low complexity, discrete-time algorithms are developed for channel estimation, carrier and timing synchronization, and finally turbo decoding of the data at the receiver. Computer simulation results are presented to validate the theory.

Keywords: 5G, channel capacity, channel estimation, single-user massive MIMO, OFDM, spatial multiplexing, retransmissions, synchronization, turbo codes

1. Introduction

The main objective of the fifth-generation [1–15] wireless communication standard is to provide peak data rates of 10 gigabit per second (Gbps) for each user, ultra-low latency (the time duration between transmission of information and getting a response) of less than 1 ms, and, last but not the least, very low bit error rates (BER) ($< 10^{-10}$). High data rates are essential for streaming ultrahigh definition (4k) video. Low latency is required for future driverless cars and remote surgeries. An important feature of the 5G network is that it involves not only people but also smart devices. For example, it may be possible to control a microwave oven or geyser located in the home, from the office. High data rates are feasible by using a large number of transmitting antennas. For example, if each transmit antenna transmits at a rate of 100 megabits per second (Mbps), then using 100 transmit antennas would result in an overall bit-rate of 10 Gbps. This technique of increasing the overall bit-rate by using a large number of transmit antennas is also known as spatial multiplexing (not to be confused with spatial modulation [16–20], wherein not all the transmit antennas are simultaneously active). This is illustrated in **Figure 1**, where the i^{th} transmit antenna sends C_i bits of information and each of the receive antennas gets C/N bits

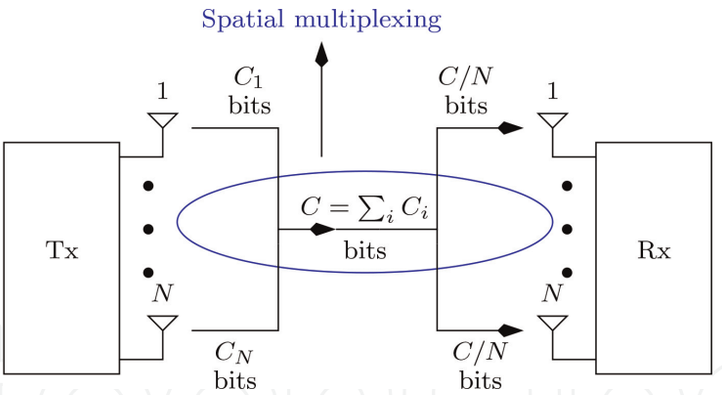

Figure 1.
Illustration of spatial multiplexing for $N \times N$ MIMO.

of information, in each transmission (see *Proposition A.1* and *A.2* in [21]). It must be noted that a large array of transmit antennas can also be used for beamforming [22, 23] and beam steering (the ability to focus the transmitted signal in a particular direction, without moving the antenna), which is not the topic of this chapter. In fact, the basic idea used in this chapter is captured in the following proposition.

Proposition 1.1 *Signals transmitted and received by antennas separated by at least $\lambda/2$ ($\lambda = c/\nu$ where c is the velocity of light and ν is the carrier frequency) undergo independent fading.*

A typical massive MIMO antenna array is shown in **Figure 2**. The black dots denote the antennas, and the circles denote obstructions used to prevent mutual coupling between the antennas. While spatial multiplexing is a big advantage in massive MIMO, the main problem lies in the high complexity of data detection at the receiver. To understand this issue, consider the signal model:

$$\tilde{\mathbf{R}} = \tilde{\mathbf{H}}\mathbf{S} + \tilde{\mathbf{W}} \tag{1}$$

where $\tilde{\mathbf{R}} \in \mathbb{C}^{N\times 1}$ is the received vector, $\tilde{\mathbf{H}} \in \mathbb{C}^{N\times N}$ is the channel matrix, $\mathbf{S} \in \mathbb{C}^{N\times 1}$ is the symbol vector drawn from an M-ary 2D constellation, and $\tilde{\mathbf{W}} \in \mathbb{C}^{N\times 1}$ is the

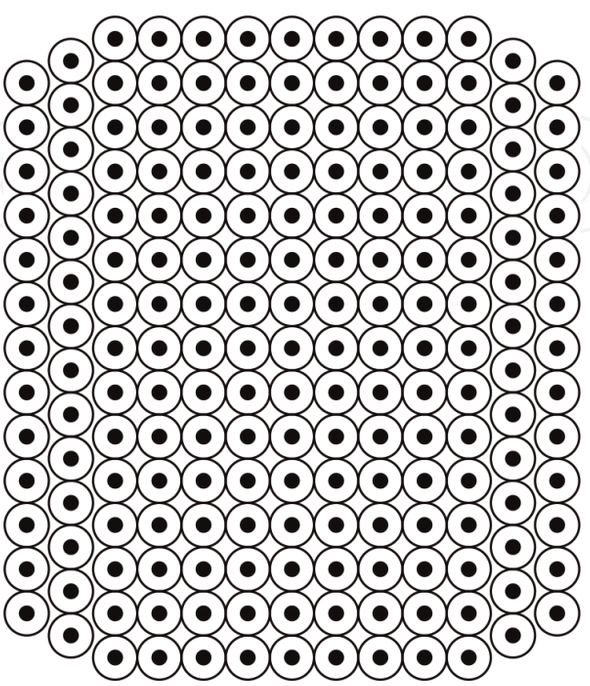

Figure 2.
A massive MIMO antenna array.

additive white Gaussian noise (AWGN) vector. Here $\mathbb{C}$ denotes the set of complex numbers. Due to Proposition 1.1, the elements of $\tilde{\mathbf{H}}$ are statistically independent. Moreover, if there is no line-of-sight (LOS) path between the transmitter and receiver, the elements of $\tilde{\mathbf{H}}$ are zero-mean Gaussian. The elements of $\tilde{\mathbf{W}}$ are also assumed to be independent. The real and imaginary parts of the elements of $\tilde{\mathbf{H}}$ and $\tilde{\mathbf{W}}$ are also assumed to be independent. Now, the problem statement is find $\mathbf{S}$ given $\tilde{\mathbf{R}}$. There are several methods of solving this problem, assuming that $\tilde{\mathbf{H}}$ is known.

1. Perform an exhaustive search over all the M^N possibilities of $\mathbf{S}$. This is known as the maximum likelihood (ML) approach, which has got an exponential complexity.

2. Pre-multiply $\tilde{\mathbf{R}}$ with $\tilde{\mathbf{H}}^{-1}$. This is known as the zero-forcing approach and has a complexity of the order of $2N^3$ (N^3 complexity for computing the inverse and another N^3 for matrix multiplication). This approach usually leads to noise enhancement and a poor symbol error rate (SER) performance.

3. The third approach, known as sphere decoding, has polynomial complexity ($\sim C_0 \times N^{C_1}$, where C_0>1 and C_1>3) and has been widely studied in the literature [24–33].

Data detection in single-user massive MIMO systems using retransmissions, having a complexity of $N_{rt} \times N^3$, where N_{rt} is the number of retransmissions, has been proposed [34], where it was assumed that $\tilde{\mathbf{H}}$ is known at the receiver. In this work, which is an extension of [34], we present a coherent receiver for massive MIMO systems, where not only $\tilde{\mathbf{H}}$ but also the carrier frequency offset and timing are estimated. Moreover, the signal model in Eq. (1) is valid for flat fading channels. When the channel is frequency selective (the length of the discrete-time channel impulse response is greater than unity), orthogonal frequency division multiplexing needs to be used, since OFDM converts a frequency-selective channel into a flat fading channel (length of the discrete-time channel impulse response is equal to unity) [35]. To this end, the channel estimation and carrier and timing synchronization algorithms developed in [36] for single-input single-output (SISO) OFDM, [37, 38] for single-input multiple-output (SIMO) OFDM, and [21, 39] for multiple-input multiple-output (MIMO) OFDM are used in this work. In [40], a linear prediction-based detection of serially concatenated QPSK is presented, which does not require any preamble. The prospect of using superimposed training [41] in the context of massive MIMO looks quite intimidating, since the signal at each receive antenna is already a superposition of the signals from a large number of transmit antennas.

This work is organized as follows. Section 2 presents the system model. The discrete-time receiver algorithms are presented in Section 3. The computer simulation results are discussed in Section 4, and the chapter concludes with Section 5.

2. System model

The transmitted frame structure is shown in **Figure 3(a)**. The signal in the blue boxes is sent from transmit antenna n_t. The signal in the red boxes is sent from other antennas. Note that in the preamble phase, only one transmit antenna is active at a time, whereas in the data phase, all transmit antennas are active simultaneously. In

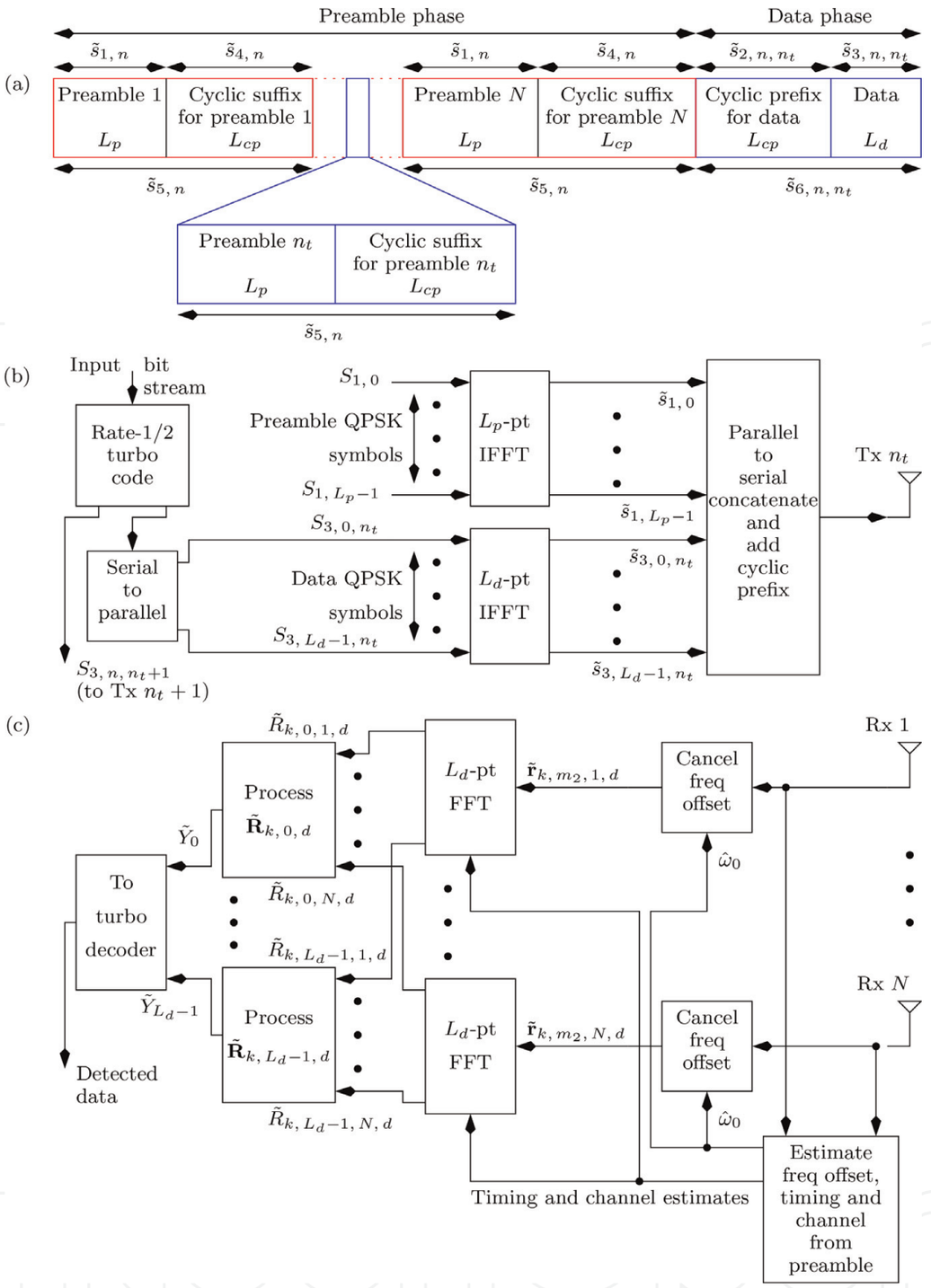

Figure 3.
(a) Frame structure for k^{th} retransmission. (b) Signal from transmit antenna n_t. (c) Receiver for the data phase.

practice, each transmit antenna could use a different preamble. However, in this work, we assume that all transmit antennas use the same preamble. The signals in **Figure 3(a)** are defined as follows (similar to [21]):

$$\begin{aligned}
\tilde{s}_{1,n} &= \frac{1}{L_p}\sum_{i=0}^{L_p-1} S_{1,i} e^{j2\pi ni/L_p} \quad \text{for } 0 \le n \le L_p - 1 \\
\tilde{s}_{3,n,n_t} &= \frac{1}{L_d}\sum_{i=0}^{L_d-1} S_{3,i,n_t} e^{j2\pi ni/L_d} \quad \text{for } 0 \le n \le L_d - 1 \\
\tilde{s}_{2,n,n_t} &= \tilde{s}_{3,L_d-L_{cp}+n,n_t} \quad \text{for } 0 \le n \le L_{cp} - 1 \\
\tilde{s}_{4,n} &= \tilde{s}_{1,n} \quad \text{for } 0 \le n \le L_{cp} - 1.
\end{aligned} \tag{2}$$

The term i in the above equations denotes the i^{th} subcarrier, n denotes the time index, and $1 \le n_t \le N$ is the index to the transmit antenna. Note that in this work, the same preamble is transmitted one after the other by each of the transmit antennas, as shown in **Figure 3(a)**. In [21], different preambles are transmitted simultaneously from all the transmit antennas. The channel coefficients $\tilde{h}_{k,n,n_r,n_t}$ associated with the receive antenna n_r $(1 \le n_r \le N)$ and transmit antenna n_t $(1 \le n_t \le N)$ for the k^{th} retransmission are $\mathcal{CN}\left(0, 2\sigma_f^2\right)$ ($\mathcal{CN}(\cdot)$ denotes a circularly symmetric Gaussian random variable) and satisfy the following relations [21]:

$$\begin{aligned}
\frac{1}{2}E\left[\tilde{h}_{k,n,n_r,n_t}\tilde{h}^*_{k,m,n_r,n_t}\right] &= \sigma_f^2\delta_K(n-m)\\
\frac{1}{2}E\left[\tilde{h}_{k,n,n_r,n_t}\tilde{h}^*_{k,n,m_r,n_t}\right] &= \sigma_f^2\delta_K(n_r-m_r)\\
\frac{1}{2}E\left[\tilde{h}_{k,n,n_r,n_t}\tilde{h}^*_{k,n,n_r,m_t}\right] &= \sigma_f^2\delta_K(n_t-m_t)\\
\frac{1}{2}E\left[\tilde{h}_{k,n,n_r,n_t}\tilde{h}^*_{i,n,n_r,n_t}\right] &= \sigma_f^2\delta_K(k-i)
\end{aligned} \tag{3}$$

where "*" denotes complex conjugate and $\delta_K(\cdot)$ is the Kronecker delta function. Observe that Eq. (3) implies a uniform power delay profile. Even though an exponential power delay profile is more realistic, we have used a uniform power delay profile, since it is expected to give the worst-case BER performance, as all the multipath components have the same power [21]. The channel is assumed to be quasi-static, that is, $\tilde{h}_{k,n,n_r,n_t}$ is time-invariant over one frame (retransmission). The length of all the N^2 channel impulse responses is assumed to be L_h, which is proportional to the difference between the longest and shortest multipath [21]. The channel span assumed by the receiver is [21, 36, 39].

$$L_{hr} = 2L_h - 1. \tag{4}$$

The length of the cyclic prefix or suffix is [21, 36, 39].

$$L_{cp} = L_{hr} - 1. \tag{5}$$

The length of the preamble is L_p, and the length of the data is L_d. The AWGN noise samples $\tilde{w}_{k,n,n_r}$ for the k^{th} retransmission at time n and receive antenna n_r are $\mathcal{CN}\left(0, 2\sigma_w^2\right)$ and satisfy

$$\begin{aligned}
\frac{1}{2}E\left[\tilde{w}_{k,n,n_r}\tilde{w}^*_{k,m,n_r}\right] &= \sigma_w^2\delta_K(n-m)\\
\frac{1}{2}E\left[\tilde{w}_{k,n,n_r}\tilde{w}^*_{k,n,m_r}\right] &= \sigma_w^2\delta_K(n_r-m_r)\\
\frac{1}{2}E\left[\tilde{w}_{k,n,n_r}\tilde{w}^*_{i,m,n_r}\right] &= \sigma_w^2\delta_K(k-i).
\end{aligned} \tag{6}$$

The noise and channel coefficients are assumed to be independent. The frequency offset ω_0 is uniformly distributed over $[-0.03, 0.03]$ radians, and the ML frequency offset estimator searches in the range $[-\omega_{0,\max}, \omega_{0,\max}]$ radians [42] where

$$\omega_{0,\max} = 0.04\,radian. \tag{7}$$

For convenience, and without loss of generality, we assume that ω_0 is constant over N_{rt} retransmissions.

During the preamble phase, the signal at receive antenna n_r, for the k^{th} retransmission, can be written as (for $0 \le n \le L_p + L_{cp} + L_h - 2$)

$$\begin{aligned}\tilde{r}_{k,n,n_r,n_t,p} &= \left(\tilde{s}_{5,n} \star \tilde{h}_{k,n,n_r,n_t}\right) \mathrm{e}^{\mathrm{j}\omega_0 n} + \tilde{w}_{k,n,n_r,n_t,p} \\ &= \tilde{y}_{k,n,n_r,n_t,p} \mathrm{e}^{\mathrm{j}\omega_0 n} + \tilde{w}_{k,n,n_r,n_t,p}\end{aligned} \tag{8}$$

where "$\star$" denotes linear convolution, $\tilde{s}_{5,n}$ is depicted in **Figure 3(a)**, $\tilde{h}_{k,n,n_r,n_t}$ denotes the channel impulse response between transmit antenna n_t and receive antenna n_r for the k^{th} retransmission, and

$$\tilde{y}_{k,n,n_r,n_t,p} = \tilde{s}_{5,n} \star \tilde{h}_{k,n,n_r,n_t}. \tag{9}$$

The subscript "p" in Eqs. (8) and (9) denotes the preamble. Note that any random carrier phase can be absorbed in the channel impulse response. We have

$$\begin{aligned}\tilde{s}_{1,n} \odot_{L_p} \tilde{s}^*_{1,-n} &= E_s \delta_K(n) \\ &\overset{L_p}{\rightleftharpoons} \left|\tilde{S}_{1,i}\right|^2 \\ &= \text{a constant for } 0 \le i \le L_p - 1\end{aligned} \tag{10}$$

where "$\odot_{L_p}$" denotes an L_p-point circular convolution, "$\overset{L_p}{\rightleftharpoons}$" denotes the L_p-point discrete Fourier transform (DFT) or the fast Fourier transform (FFT), and

$$E_s = \sum_{n=0}^{L_p-1} \left|\tilde{s}_{1,n}\right|^2. \tag{11}$$

Due to the presence of the cyclic suffix, we have

$$\tilde{s}_{5,n} \star \tilde{s}^*_{1,-n} \begin{cases} = 0 & \text{for } 1 \le n \le L_{hr} - 1 \\ = E_s & \text{for } n = 0 \\ \ll E_s & \text{otherwise.} \end{cases} \tag{12}$$

Assuming perfect carrier and timing synchronization (ω_0 is perfectly canceled and the frame boundaries are perfectly known) at the receiver, the signal at the output of the L_p-point FFT for the i^{th} ($0 \le i \le L_p - 1$) subcarrier and receive antenna n_r, due to the preamble sent from transmit antenna n_t during the k^{th} retransmission, is

$$\tilde{R}_{k,i,n_r,n_t,p} = \tilde{H}_{k,i,n_r,n_t} S_{1,i} + \tilde{W}_{k,i,n_r,n_t,p} \tag{13}$$

where $\tilde{H}_{k,i,n_r,n_t}$ and $\tilde{W}_{k,i,n_r,n_t,p}$ denote the L_p-point FFT of $\tilde{h}_{k,n,n_r,n_t}$ and $\tilde{w}_{k,n,n_r,n_t,p}$, respectively. The average SNR per bit corresponding to Eq. (13) is

$$\begin{aligned} SNR_{\text{av},b,p} &= \frac{E\left[2A^2\left|\tilde{H}_{k,i,n_r,n_t}\right|^2\right]}{E\left[\left|\tilde{W}_{k,i,n_r,n_t,p}\right|^2\right]} \times \frac{NN_{rt}}{2} \\ &= \frac{2A^2\left(2L_h\sigma_f^2\right)NN_{rt}}{\left(2L_p\sigma_w^2\right)\times 2} \\ &= \frac{A^2L_h\sigma_f^2NN_{rt}}{L_p\sigma_w^2} \end{aligned} \tag{14}$$

where [36]

$$\begin{aligned} E\left[\left|\tilde{H}_{k,i,n_r,n_t}\right|^2\right] &= 2L_h\sigma_f^2 \\ E\left[\left|\tilde{W}_{k,i,n_r,n_t,p}\right|^2\right] &= 2L_p\sigma_w^2 \\ E\left[\left|S_{1,i}\right|^2\right] &\triangleq 2A^2 \\ &= E_s \end{aligned} \tag{15}$$

where A is a constant to be determined and it is assumed that each sample of each receive antenna gets $2/(NN_{rt})$ bits of information during the preamble phase (see *Proposition A.2* in [21]).

During the data phase, the signal for the k^{th} retransmission at receive antenna n_r can be written as (for $0 \le n \le L_d + L_{cp} + L_h - 2$)

$$\begin{aligned} \tilde{r}_{k,n,n_r,d} &= \sum_{n_t=1}^{N}\left(\tilde{s}_{6,n,n_t} \star \tilde{h}_{k,n,n_r,n_t}\right)e^{j\omega_0 n} + \tilde{w}_{k,n,n_r,d} \\ &= \tilde{y}_{k,n,n_r,d}e^{j\omega_0 n} + \tilde{w}_{k,n,n_r,d} \end{aligned} \tag{16}$$

where $\tilde{s}_{6,n,n_t}$ is depicted in **Figure 3(a)** and

$$\tilde{y}_{k,n,n_r,d} = \sum_{n_t=1}^{N}\tilde{s}_{6,n,n_t} \star \tilde{h}_{k,n,n_r,n_t}. \tag{17}$$

The subscript "d" in Eqs. (16) and (17) denotes data. Assuming perfect carrier and timing synchronization at the receiver, the signal at the output of the L_d-point FFT for the i^{th} $(0 \le i \le L_d - 1)$ subcarrier and receive antenna n_r, during the k^{th} retransmission, is

$$\tilde{R}_{k,i,n_r,d} = \sum_{n_t=1}^{N}\tilde{H}_{k,i,n_r,n_t}S_{3,i,n_t} + \tilde{W}_{k,i,n_r,d} \tag{18}$$

where $\tilde{H}_{k,i,n_r,n_t}$ and $\tilde{W}_{k,i,n_r,d}$ denote the L_d-point FFT of $\tilde{h}_{k,n,n_r,n_t}$ and $\tilde{w}_{k,n,n_r,d}$, respectively. The average SNR per bit corresponding to Eq. (18) is

$$
\begin{aligned}
SNR_{\text{av},b,d} &= \frac{E\left[\left|\sum_{n_t=1}^{N}\tilde{H}_{k,i,n_r,n_t}S_{3,i,n_t}\right|^2\right]}{E\left[\left|\tilde{W}_{k,i,n_r,d}\right|^2\right]}\times 2N_{rt} \\
&= \frac{2\left(2L_h\sigma_f^2\right)N(2N_{rt})}{2L_d\sigma_w^2} \\
&= \frac{4L_h\sigma_f^2NN_{rt}}{L_d\sigma_w^2}
\end{aligned}
\tag{19}
$$

where [36].

$$
\begin{aligned}
E\left[\left|\tilde{W}_{k,i,n_r,d}\right|^2\right] &= 2L_d\sigma_w^2 \\
E\left[\left|S_{3,i,n_t}\right|^2\right] &\triangleq 2
\end{aligned}
\tag{20}
$$

and it is assumed that each receive antenna gets $1/(2N_{rt})$ bits of information in each transmission [34]. We impose the constraint that

$$
\begin{aligned}
\text{SNR}_{\text{av},b,p} &= \text{SNR}_{\text{av},b,d} \\
\Rightarrow \frac{A^2L_h\sigma_f^2NN_{rt}}{L_p\sigma_w^2} &= \frac{4L_h\sigma_f^2NN_{rt}}{L_d\sigma_w^2} \\
\Rightarrow A &= \sqrt{\frac{4L_p}{L_d}}.
\end{aligned}
\tag{21}
$$

Let us now compare the average power of the preamble with that of the data, at the transmitter. The average power of the preamble in the time domain is

$$
\begin{aligned}
E\left[\left|\tilde{s}_{1,n}\right|^2\right] &= \frac{1}{L_p^2}E\left[\sum_{i=0}^{L_p-1}S_{1,i}e^{j2\pi ni/L_p}\sum_{l=0}^{L_p-1}S_{1,l}^{*}e^{-j2\pi nl/L_p}\right] \\
&= \frac{1}{L_p^2}\sum_{i=0}^{L_p-1}\sum_{l=0}^{L_p-1}E\left[S_{1,i}S_{1,l}^{*}\right]\times e^{-j2\pi n(i-l)/L_p} \\
&= \frac{1}{L_p^2}\sum_{i=0}^{L_p-1}\sum_{l=0}^{L_p-1}2A^2\delta_K(i-l)\times e^{-j2\pi n(i-l)/L_p} \\
&= \frac{2A^2}{L_p} \\
&= \frac{8}{L_d}
\end{aligned}
\tag{22}
$$

where A is defined in Eqs. (15) and (21). Similarly, the average power of the data in the time domain is

$$
E\left[\left|\tilde{s}_{3,n,n_t}\right|^2\right] = \frac{2}{L_d}. \tag{23}
$$

Therefore, the radio frequency (RF) amplifiers at the transmitter must have a dynamic range of at least (note that the RF amplifiers have to also deal with the peak-to-average power ratio (PAPR) problem [43–49])

$$\begin{aligned} 10\log_{10}\left(\frac{E\left[|\tilde{s}_{1,n}|^2\right]}{E\left[|\tilde{s}_{3,n,n_t}|^2\right]}\right) &= 10\log_{10}(4)\ \text{dB} \\ &= 6\ \text{dB}. \end{aligned} \tag{24}$$

Let us now consider the case where the preamble power is equal to the data power at each transmit antenna. From Eqs. (22) and (23), we have [36]

$$\begin{aligned} \frac{2A^2}{L_p} &= \frac{2}{L_d} \\ \Rightarrow A &= \sqrt{\frac{L_p}{L_d}}. \end{aligned} \tag{25}$$

Substituting for A from Eq. (25), we obtain the average SNR per bit of the preamble phase and the data phase as

$$\begin{aligned} \text{SNR}_{\text{av},b,p} &= \frac{A^2 L_h \sigma_f^2 N N_{rt}}{L_p \sigma_w^2} \\ &= \frac{L_h \sigma_f^2 N N_{rt}}{L_d \sigma_w^2} \\ \text{SNR}_{\text{av},b,d} &= \frac{4 L_h \sigma_f^2 N N_{rt}}{L_d \sigma_w^2} \\ \Rightarrow\ 10\log_{10}\left(\frac{\text{SNR}_{\text{av},b,d}}{\text{SNR}_{\text{av},b,p}}\right) &= 10\log_{10}(4)\ \text{dB}. \\ &= 6\ \text{dB}. \end{aligned} \tag{26}$$

In other words, the average SNR per bit of the preamble phase would be less than that of the data phase by 6 dB. In what follows, we assume that A is given by (21).

3. Receiver algorithms

The receiver algorithms have been adapted from [21, 36, 37, 39] and will be briefly described in the following subsections.

3.1 Start of frame and frequency offset estimation

The first task of the receiver is to detect the presence of a valid signal, that is, the start of frame (SoF). The SoF detection and coarse frequency offset estimation are performed for each receive antenna $1 \le n_r \le N$, transmit antenna $1 \le n_t \le N$, and retransmission $1 \le k \le N_{rt}$ as given by the following rule (similar to Eq. (17) in [21]: choose that value of $\hat{m}_k(n_r, n_t)$ and $\hat{\nu}_k(n_r, n_t)$ which maximizes

$$\left| \left(\tilde{r}_{k,m,n_r,n_t,p} \, \mathrm{e}^{-\mathrm{j}\hat{\nu}_k}(n_r,n_t)m \right) \star \tilde{s}^*_{1,L_p-1-m,n_t} \right| \tag{27}$$

where $\tilde{r}_{k,m,n_r,n_t,p}$ is given in Eq. (8) and

$$\hat{\nu}_k(n_r,n_t) \in \left\{ -\omega_{0,\max} + \frac{2l\omega_{0,\max}}{B_1} \right\} \tag{28}$$

for $0 \le l \le B_1$, where l and B_1 [21] are positive integers and $\omega_{0,\max}$ is given in Eq. (7). Observe that $\hat{m}_k(n_r,n_t)$ satisfies Eqs. (18) and (19) in [21]. The average value of the frequency offset estimate is given by

$$\hat{\omega}_0 = \frac{\sum_{k=1}^{N_{rt}} \sum_{n_r=}^{N} \sum_{n_t=1}^{N} \hat{\nu}_k(n_r,n_t)}{N^2 N_{rt}}. \tag{29}$$

3.2 Channel estimation

We assume that the SoF has been estimated using Eq. (27) with outcome m_0 given by (assuming the condition (19) in [21] is satisfied for all k, n_r, and n_t)

$$m_0 = \hat{m}_1(1,1) - L_p + 1 \quad 0 \;\le\; m_0 \le\; L_h \;\; - 1 \tag{30}$$

and the frequency offset has been perfectly canceled [36, 38]. Observe that any value of k, n_r, and n_t can be used in the computation of Eq. (30). We have taken $k = n_r = n_t = 1$. Define [21, 36, 39].

$$m_1 = m_0 + L_h - 1. \tag{31}$$

The steady-state, preamble part of the received signal for the k^{th} retransmission and receive antenna n_r can be written as [21, 36, 39]

$$\tilde{\mathbf{r}}_{k,m_1,n_r,n_t,p} = \tilde{\mathbf{s}}_5 \tilde{\mathbf{h}}_{k,n_r,n_t} + \tilde{\mathbf{w}}_{k,m_1,n_r,n_t,p} \tag{32}$$

where

$$\begin{aligned}
\tilde{\mathbf{r}}_{k,m_1,n_r,n_t,p} &= \left[\tilde{r}_{k,m_1,n_r,n_t,p} \;\; \cdots \;\; \tilde{r}_{k,m_1+L_p-1,n_r,n_t,p} \right]^T_{L_p \times 1} \\
\tilde{\mathbf{w}}_{k,m_1,n_r,n_t,p} &= \left[\tilde{w}_{k,m_1,n_r,n_t,p} \;\; \cdots \;\; \tilde{w}_{k,m_1+L_p-1,n_r,n_t,p} \right]^T_{L_p \times 1} \\
\tilde{\mathbf{h}}_{k,n_r,n_t} &= \left[\tilde{h}_{k,0,n_r,n_t} \;\; \cdots \;\; \tilde{h}_{k,L_{hr}-1,n_r,n_t} \right]^T_{L_{hr} \times 1} \\
\tilde{\mathbf{s}}_5 &= \begin{bmatrix} \tilde{s}_{5,L_{hr}-1} & \cdots & \tilde{s}_{5,0} \\ \vdots & \cdots & \vdots \\ \tilde{s}_{5,L_p+L_{hr}-2} & \cdots & \tilde{s}_{5,L_p-1} \end{bmatrix}_{L_p \times L_{hr}}.
\end{aligned} \tag{33}$$

Observe that $\tilde{\mathbf{s}}_5$ is independent of m_1 and due to the relations in Eqs. (10), (15), and (21), we have

$$\tilde{\mathbf{s}}_5^H \tilde{\mathbf{s}}_5 = \frac{8L_p}{L_d} \mathbf{I}_{L_{hr}}. \tag{34}$$

where $\mathbf{I}_{L_{hr}}$ is an $L_{hr} \times L_{hr}$ identity matrix. The estimate of the channel is [21, 36, 39]

$$\hat{\mathbf{h}}_{k,n_r,n_t} = \left(\tilde{\mathbf{s}}_5^H \tilde{\mathbf{s}}_5\right)^{-1} \tilde{\mathbf{s}}_5^H \tilde{\mathbf{r}}_{k,m_1,n_r,n_t,p}. \tag{35}$$

To see the effect of noise on the channel estimate in Eq. (35), consider

$$\tilde{\mathbf{u}} = \left(\tilde{\mathbf{s}}_5^H \tilde{\mathbf{s}}_5\right)^{-1} \tilde{\mathbf{s}}_5^H \tilde{\mathbf{w}}_{k,m_1,n_r,n_t,p}. \tag{36}$$

It can be shown that [21, 39]

$$E\left[\tilde{\mathbf{u}}\tilde{\mathbf{u}}^H\right] = \frac{\sigma_w^2 L_d}{4L_p} \mathbf{I}_{L_{hr}} \triangleq 2\sigma_u^2 \mathbf{I}_{L_{hr}}. \tag{37}$$

3.3 Noise variance estimation

The noise variance per dimension is estimated as

$$\begin{aligned}\hat{\sigma}_w^2 = \frac{1}{2L_p N^2 N_{rt}} \sum_{k=1}^{N_{rt}} \sum_{n_t=1}^{N} \sum_{n_r=1}^{N} \left(\tilde{\mathbf{r}}_{k,m_1,n_r,n_t,p} - \tilde{\mathbf{s}}_5 \hat{\mathbf{h}}_{k,n_r,n_t}\right)^H \\ \left(\tilde{\mathbf{r}}_{k,m_1,n_r,n_t,p} - \tilde{\mathbf{s}}_5 \hat{\mathbf{h}}_{k,n_r,n_t}\right).\end{aligned} \tag{38}$$

3.4 Post-FFT operations

In this section, we assume that the residual frequency offset given by

$$\omega_r = \omega_0 - \hat{\omega}_0 \tag{39}$$

is such that

$$\omega_r L_d < 0.1 \quad \text{radians} \tag{40}$$

so that the effect of inter carrier interference (ICI) is negligible. Let

$$m_2 = m_1 + N\left(L_p + L_{cp}\right) \tag{41}$$

where m_1 is defined in Eq. (31). Note that m_2 is the starting point of the data phase. Define the FFT input in the time domain for the k^{th} retransmission and receive antenna n_r as

$$\tilde{\mathbf{r}}_{k,m_2,n_r,d} = \left[\tilde{r}_{k,m_2,n_r,d} \quad \ldots \quad \tilde{r}_{k,m_2+L_d-1,n_r,d}\right]_{L_d \times 1}^T \tag{42}$$

where we have followed the notation in Eq. (16). The L_d-point FFT of Eq. (42) is

$$\tilde{\mathbf{R}}_{k,n_r,d} = \left[\tilde{R}_{k,0,n_r,d} \quad \ldots \quad \tilde{R}_{k,L_d-1,n_r,d}\right]_{L_d \times 1}^T \tag{43}$$

where $\tilde{R}_{k,i,n_r,d}$ is given by Eq. (18). Construct a matrix:

$$\tilde{\mathbf{R}}_{k,i,d} = \left[\tilde{R}_{k,i,1,d} \quad \ldots \quad \tilde{R}_{k,i,N,d}\right]_{N \times 1} \tag{44}$$

for $0 \le i \le L_d - 1$. Note that from Eq. (18)

$$\tilde{\mathbf{R}}_{k,i,d} = \tilde{\mathbf{H}}_{k,i}\mathbf{S}_{3,i} + \tilde{\mathbf{W}}_{k,i,d} \tag{45}$$

where

$$\begin{aligned}
\tilde{\mathbf{H}}_{k,i} &= \begin{bmatrix} \tilde{H}_{k,i,1,1} & \dots & \tilde{H}_{k,i,1,N} \\ \vdots & \dots & \vdots \\ \tilde{H}_{k,i,N,1} & \dots & \tilde{H}_{k,i,N,N} \end{bmatrix}_{N\times N} \\
\mathbf{S}_{3,i} &= [\, S_{3,i,1} \quad \dots \quad S_{3,i,N} \,]^T_{N\times 1} \\
\tilde{\mathbf{W}}_{k,i,d} &= [\, \tilde{W}_{k,i,1,d} \quad \dots \quad \tilde{W}_{k,i,N,d} \,]^T_{N\times 1}.
\end{aligned} \tag{46}$$

which is similar to Eq. (1) in [34]. Let

$$\tilde{\mathbf{Y}}_{k,i} = \hat{\mathbf{H}}^H_{k,i}\tilde{\mathbf{R}}_{k,i,d} = \hat{\mathbf{H}}^H_{k,i}\tilde{\mathbf{H}}_{k,i}\mathbf{S}_{3,i} + \hat{\mathbf{H}}^H_{k,i}\tilde{\mathbf{W}}_{k,i,d} \tag{47}$$

where $\hat{\mathbf{H}}_{k,i}$ is constructed from the L_d-point FFT of $\hat{\mathbf{h}}_{k,n_r,n_t}$ in Eq. (35) and $\hat{\mathbf{Y}}_{k,i}$ is similar to $\tilde{\mathbf{Y}}_k$ in Eq. (6) of [34]. The analysis when

$$\hat{\mathbf{H}}_{k,i} = \tilde{\mathbf{H}}_{k,i} \tag{48}$$

is given in [34]. Let

$$\tilde{\mathbf{Y}}_i = \frac{1}{N_{rt}}\sum_{k=1}^{N_{rt}} \tilde{\mathbf{Y}}_{k,i} \qquad \text{for } 0 \le i \le L_d - 1. \tag{49}$$

Note that $\tilde{\mathbf{Y}}_i$ is an $N \times 1$ matrix, whose n_t^{th} element $\tilde{Y}_{i,n_t}$ is a noisy version of S_{3,i,n_t} in Eq. (18). The matrix

$$\tilde{\mathbf{Y}}_{n_t} = \left[\, \tilde{Y}_{0,n_t} \dots \tilde{Y}_{L_d-1,n_t} \,\right]^T_{L_d\times 1} \tag{50}$$

constructed from the elements of $\tilde{\mathbf{Y}}_i$ in Eq. (49) is fed to the turbo decoder. The forward (α) backward (β) recursions for decoder 1 of the turbo code is given by Eqs. (28) and (31) in [34]. The term $\gamma_{1,i,m,n}$ in Eq. (30) of [34] should be replaced by

$$\gamma_{1,i,m,n,n_t} = \exp\left[-\frac{\left|\tilde{Y}_{i,n_t} - F_{i,n_t}S_{m,n}\right|^2}{2\sigma_U^2}\right] \tag{51}$$

where $\tilde{Y}_{i,n_t}$ is an element of $\tilde{\mathbf{Y}}_{n_t}$ in Eq. (50) and n_t is an odd integer. The term σ_U^2 in Eq. (51) is given by Eq. (22) in [34] which is repeated here for convenience:

$$\sigma_U^2 = \frac{1}{N_{rt}}\left(4N\sigma_H^2\sigma_W^2 + 8N(N-1)\sigma_H^4\right) \tag{52}$$

with

$$\begin{aligned}
\sigma_W^2 &= L_d\hat{\sigma}_w^2 \\
\sigma_H^2 &= \frac{1}{2N^2N_{rt}L_d}\sum_{k=1}^{N_{rt}}\sum_{i=0}^{L_d-1}\sum_{n_r=1}^{N}\sum_{n_t=1}^{N}\left|\hat{H}_{k,i,n_r,n_t}\right|^2
\end{aligned} \tag{53}$$

where $\hat{\sigma}_w^2$ is given by Eq. (38) and $\hat{H}_{k,i,n_r,n_t}$ is obtained by taking the L_d-point FFT of (35). The term F_{i,n_t} in Eq. (51) is given by

$$F_{i,n_t} = \frac{1}{N_{rt}} \sum_{k=1}^{N_{rt}} F_{k,i,n_t} \tag{54}$$

where

$$F_{k,i,n_t} = \sum_{n_r=1}^{N} \left| \hat{H}_{k,i,n_r,n_t} \right|^2. \tag{55}$$

The extrinsic information from decoder 1 to decoder 2 is computed using Eqs. (32) and (33) of [34], with $\gamma_{1,i,n,\rho^+(n)}$ replaced by $\gamma_{1,i,n,\rho^+(n),n_t}$. The equations for decoder 2 are similar, except that $\gamma_{2,i,m,n}$ in Eq. (34) of [34] should be replaced by

$$\gamma_{2,i,m,n,n_t+1} = \exp\left[-\frac{\left| \tilde{Y}_{i,n_t+1} - F_{i,n_t+1} S_{m,n} \right|^2}{2\sigma_U^2} \right] \tag{56}$$

where again n_t is an odd integer.

3.5 Throughput and spectral efficiency

Recall from **Figure 3(a)** that during the preamble phase, only one transmit antenna is active at a time, whereas during the data phase, all the transmit antennas are simultaneously active. Thus the throughput can be defined as [36, 37].

$$\mathscr{T} = \frac{NL_d/2}{N_{rt}\left[N\left(L_p + L_{cp}\right) + L_d + L_{cp}\right]}. \tag{57}$$

The numerator of Eq. (57) denotes the total number of data bits transmitted, and the denominator represents the total number of QPSK symbol *durations* over N_{rt} retransmissions. The symbol rate during the preamble phase and data phase is the same. In the data phase, we are transmitting coded QPSK, that is, in each data bit duration, two coded QPSK symbols are sent simultaneously from two transmit antennas (see **Figure 3(b)**). Thus, during the data phase, each transmit antenna sends half a bit of information in each transmission. Therefore, the spectral efficiency is

Simulation parameters		**Throughput $\mathscr{T}$**
L_p = 512		
L_d = 1024	N = 4	32.38%
L_{cp} = 18 N_{rt} = 2	N = 8	38.77%
L_p = 4096		
L_d = 8192	N = 4	33.21%
L_{cp} = 18 N_{rt} = 2	N = 8	39.84%

Table 1.
Throughput for various simulation parameters.

$$\mathscr{S} = N/(2N_{rt}) \quad \text{bits per transmission.} \tag{58}$$

The throughput for various simulation parameters is given in **Table 1**. Observe that when $L_p = L_d/2$, $L_{cp} \ll L_d$, and $N \gg 1$, $\mathscr{T} \to 1/N_{rt}$. In this work, we have used a rate-1/2 turbo code, that is, each data bit generates two coded QPSK symbols. The throughput can be doubled by using a rate-1 turbo code, obtained by puncturing.

4. Simulation results

The simulation parameters are given in **Table 2**. A "run" in **Table 2** is defined as transmitting and receiving the frame in **Figure 3(a)** over N_{rt} retransmissions. The generating matrix of each of the constituent encoders of the turbo code is given by Eq. (49) in [21]. A question might arise: how does $N = 4, 8$ correspond to a massive MIMO system, whereas in [34] N was as large as 512? The answer is in [34], an ideal massive MIMO was considered, wherein the channel, timing, and carrier frequency offset were assumed to be known, whereas in this work, the channel, timing, and carrier frequency offset are estimated. The estimation complexity and memory requirement increase as N^2, for an $N \times N$ MIMO system. For example, the memory requirement of Eq. (27) when the number of frequency bins $B_1 = 1024$ [21], preamble length $L_p = 4096$, cyclic prefix length $L_{cp} = 18$, channel length $L_h = 10$, $N = 8$ transmit and receive antennas, and $N_{rt} = 4$ retransmissions is

$$\begin{aligned} \text{memory requirement} &= \big(L_p + L_{cp} + L_h - 1\big)(B_1 + 1)N^2 N_{rt} \\ &= 1081875200 \end{aligned} \tag{59}$$

double precision values. In fact Eq. (27) is implemented using multidimensional arrays in Scilab, instead of using for loops. Note that from Eq. (8), the length of the received signal during the preamble phase is $L_p + L_{cp} + L_h - 1$. If for loops are used, the memory requirement would be

$$\begin{aligned} \text{memory requirement} &= \big(L_p + L_{cp} + L_h - 1\big)(B_1 + 1) \\ &= 4226075 \end{aligned} \tag{60}$$

double precision values, which is much less than Eq. (59); however the simulations would run much slower. Does this mean that we cannot go higher than an

Parameter	Value
L_p	512, 4096
L_d	1024, 8192
L_h	10
L_{hr}	19
L_{cp}	18
N	4, 8
N_{rt}	1, 2, 4
B_1[21]	64, 1024
Runs	10^4, 10^3

Table 2.
Simulation parameters.

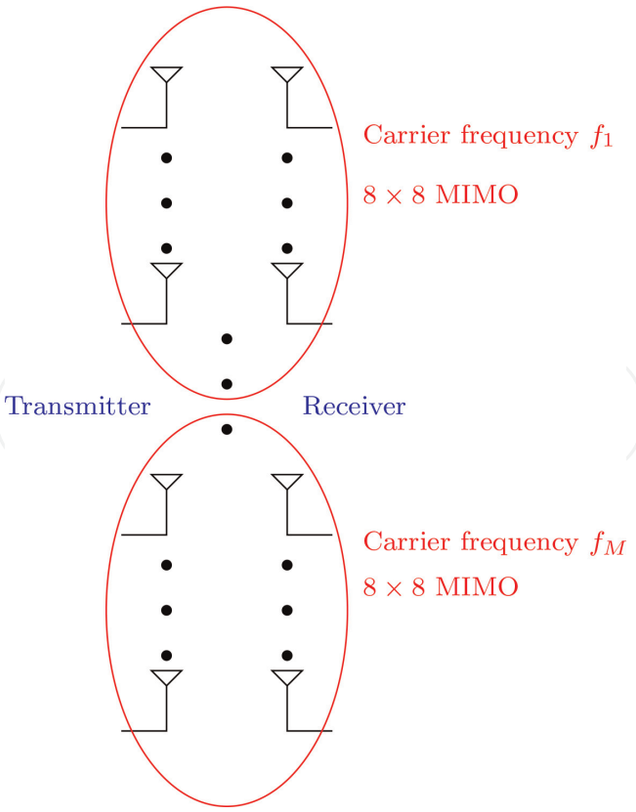

Figure 4.
Massive MIMO using multiple carrier frequencies.

8×8 MIMO system? The answer is no. The solution lies in using multiple carrier frequencies as illustrated in **Figure 4**. Observe that with 8×8 MIMO and M carrier frequencies, we get an overall $8M \times 8M$ MIMO system. The bit error rate results for a 4×4 MIMO system are shown in **Figure 5**. The bit error rate results for an 8×8 MIMO system are shown in **Figure 6**. The following observations can be made from **Figure 5**:

1. There is only 0.75 dB difference in performance between the ideal (id) and estimated (est) receiver, for $L_d = 1024$, $N_{rt} = 2$, and bit error rate equal to 10^{-4}. On the other hand, there is hardly any performance difference between the ideal and estimated receiver for $L_d = 8192$. This is because the noise

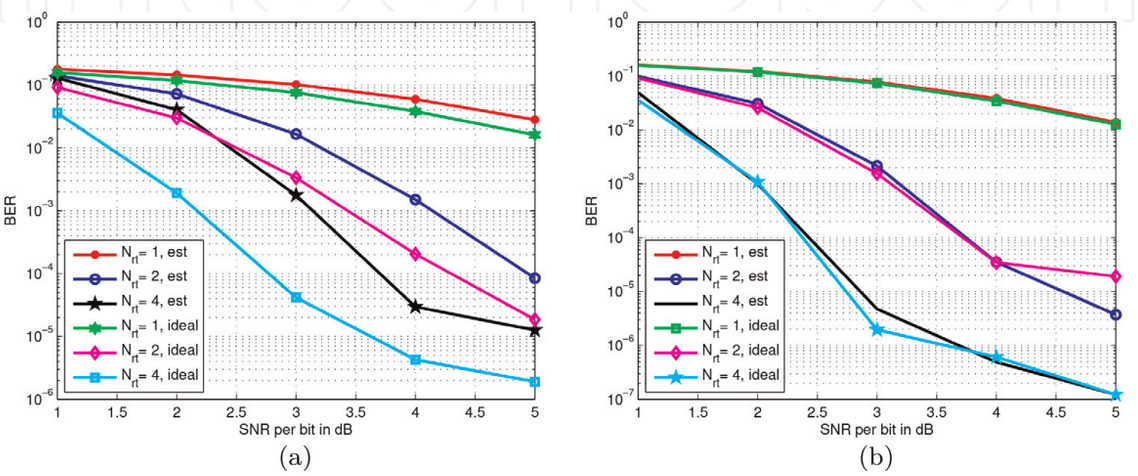

Figure 5.
Bit error rate results for a 4×4 MIMO system. (a) $L_d = 1024$ and $L_p = 512$. (b) $L_d = 8192$ and $L_p = 4096$.

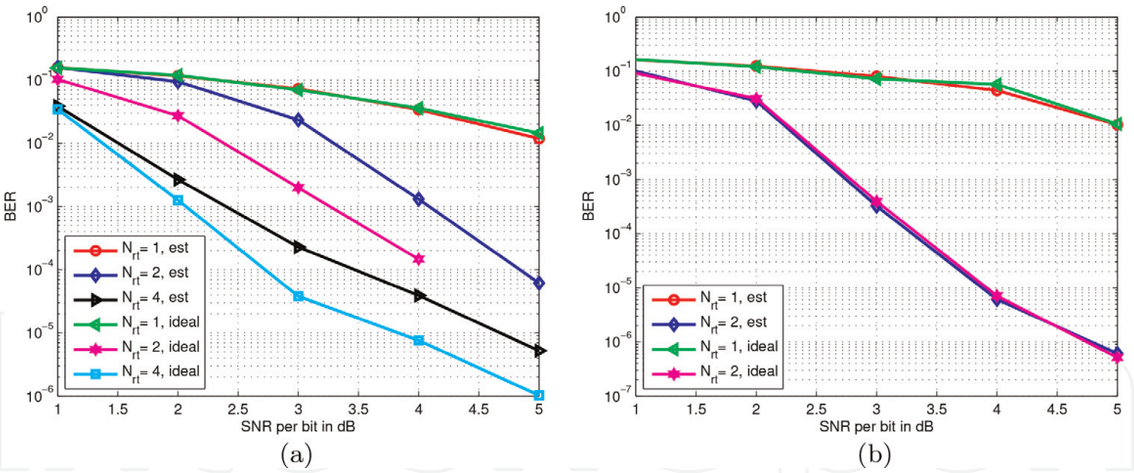

Figure 6.
Bit error rate results for an 8×8 *MIMO system. (a)* $L_d = 1024$ *and* $L_p = 512$. *(b)* $L_d = 8192$ *and* $L_p = 4096$.

variance (σ_w^2) decreases with increasing L_p, L_d, for a given average SNR per bit, as shown by Eq. (21).

2. There is only 0.5 dB improvement in performance for $L_d = 8192$ over $L_d = 1024$, at a BER of 10^{-4}.

3. There is a significant improvement in performance between $N_{rt} = 2$ and $N_{rt} = 4$, for both $L_d = 1024$ and $L_d = 8192$. On the other hand, there is no significant difference in the BER for $N_{rt} = 2$ and $N_{rt} = 4$ in [34]. The reason is because in this work, the channel $\tilde{H}_{k,i,n_r,n_t}$ in Eq. (18) is highly correlated over the subcarrier index i, since it is obtained by taking an L_d-point FFT of an L_h-tap channel (see Eq. (37) of [36]). On the other hand, the channel $\tilde{H}_{k,i,j}$ in [34] is independent over all the indices k, i, and j, where k is the retransmission index, i denotes the receive antenna index, and j denotes the transmit antenna index. See also the discussion leading to Eq. (82) in [21].

4. There is not much BER performance difference between the 4×4 and 8×8 MIMO systems. A 4×4 MIMO is computationally less complex than 8×8; however the 4×4 requires twice the number of carrier frequencies to achieve the same spectral efficiency as 8×8, for the same number of retransmissions.

5. The BER performance of the 8×8 MIMO system with $N_{rt} = 4$ and $L_d = 8192$ could not be simulated due to the large amount of memory involved (see Eq. (59)) and Scilab limitations.

5. Conclusions

This work describes the discrete-time algorithms for the implementation of a massive MIMO system. Due to the implementation complexity considerations, more than one carrier frequency is required to obtain a truly single-user massive MIMO system. Each carrier frequency needs to be associated with an 8×8 or 4×4 MIMO subsystem. The average SNR per bit has been used as a performance measure, which has not been done earlier in the literature. Perhaps the channel can also be estimated using Eq. (27), instead of using Eq. (35). This needs investigation.

Acknowledgements

The authors would like to thank the high-performance computing (HPC) facility at IIT Kanpur for running the computer simulations.

Author details

K. Vasudevan*, Shivani Singh and A. Phani Kumar Reddy
Department of Electrical Engineering, Indian Institute of Technology, Kanpur, India

*Address all correspondence to: vasu@iitk.ac.in

References

[1] Pi Z, Khan F. An introduction to millimeter-wave mobile broadband systems. IEEE Communications Magazine. 2011;**49**(6):101-107

[2] Rusek F, Persson D, Lau BK, Larsson EG, Marzetta TL, Edfors O, et al. Scaling up MIMO: Opportunities and challenges with very large arrays. IEEE Signal Processing Magazine. 2013; **30**(1):40-60

[3] Hoydis J, ten Brink S, Debbah M. Massive MIMO in the UL/DL of cellular networks: How many antennas do we need? IEEE Journal on Selected Areas in Communications. 2013;**31**(2): 160-171

[4] Rappaport TS, Sun S, Mayzus R, Zhao H, Azar Y, Wang K, et al. Millimeter wave mobile communications for 5G cellular: It will work! IEEE Access. 2013;**1**:335-349

[5] Chih-Lin I, Rowell C, Han S, Xu Z, Li G, Pan Z. Toward green and soft: A 5G perspective. IEEE Communications Magazine. 2014;**52**(2):66-73

[6] Larsson EG, Edfors O, Tufvesson F, Marzetta TL. Massive MIMO for next generation wireless systems. IEEE Communications Magazine. 2014;**52**(2): 186-195

[7] Andrews JG, Buzzi S, Choi W, Hanly SV, Lozano A, Soong ACK, et al. What will 5G be? IEEE Journal on Selected Areas in Communications. 2014;**32**(6): 1065-1082

[8] Rappaport TS, Roh W, Cheun K. Mobile's millimeter-wave makeover. IEEE Spectrum. 2014;**51**(9):34-58

[9] Marzetta TL. Massive MIMO: An introduction. Bell Labs Technical Journal. 2015;**20**:11-22

[10] Galinina O, Pyattaev A, Andreev S, Dohler M, Koucheryavy Y. 5G multi-rat LTE-WiFi ultra-dense small cells: Performance dynamics, architecture, and trends. IEEE Journal on Selected Areas in Communications. 2015;**33**(6): 1224-1240

[11] Bjrnson E, Larsson EG, Debbah M. Massive MIMO for maximal spectral efficiency: How many users and pilots should be allocated? IEEE Transactions on Wireless Communications. 2016; **15**(2):1293-1308

[12] Chih-Lin I, Han S, Xu Z, Wang S, Sun Q, Chen Y. New paradigm of 5G wireless internet. IEEE Journal on Selected Areas in Communications. 2016;**34**(3):474-482

[13] Agiwal M, Roy A, Saxena N. Next generation 5G wireless networks: A comprehensive survey. IEEE Communication Surveys and Tutorials. 2016;**18**(3):1617-1655

[14] Wong KL, Tsai CY, Lu JY, Chian DM, Li WY. Compact eight MIMO antennas for 5G smartphones and their MIMO capacity verification. In: 2016 URSI Asia-Pacific Radio Science Conference (URSI AP-RASC); 2016. pp. 1054-1056

[15] Buzzi S, D'Andrea C. Doubly massive mmWave MIMO systems: Using very large antenna arrays at both transmitter and receiver. In: 2016 IEEE Global Communications Conference (GLOBECOM); 2016. pp. 1-6

[16] Mesleh RY, Haas H, Sinanovic S, Ahn CW, Yun S. Spatial modulation. IEEE Transactions on Vehicular Technology. 2008;**57**(4):2228-2241

[17] Renzo MD, Haas H, Grant PM. Spatial modulation for multiple-antenna

wireless systems: A survey. IEEE Communications Magazine. 2011; **49**(12):182-191

[18] Renzo MD, Haas H, Ghrayeb A, Sugiura S, Hanzo L. Spatial modulation for generalized MIMO: Challenges, opportunities, and implementation. Proceedings of the IEEE. 2014;**102**(1): 56-103

[19] Cao Y, Ohtsuki T, Jiang X. Precoding aided generalized spatial modulation with an iterative greedy algorithm. IEEE Access. 2018;**6**: 72449-72457

[20] Pan Z, Luo J, Lei J, Wen L, Tang C. Uplink spatial modulation SCMA system. IEEE Communications Letters. 2019;**23.1**:184-187

[21] Vasudevan K. Near capacity signaling over fading channels using coherent turbo coded OFDM and massive MIMO. International Journal on Advances in Telecommunications. 2017; **10**(1 & 2):22-37

[22] Godara LC. Application of antenna arrays to mobile communications. II. Beam-forming and direction-of-arrival considerations. Proceedings of the IEEE. 1997;**85**(8):1195-1245

[23] Roh W, Seol JY, Park J, Lee B, Lee J, Kim Y, et al. Millimeter-wave beamforming as an enabling technology for 5G cellular communications: Theoretical feasibility and prototype results. IEEE Communications Magazine. 2014;**52**(2):106-113

[24] Vikalo H, Hassibi B, Kailath T. Iterative decoding for mimo channels via modified sphere decoding. IEEE Transactions on Wireless Communications. 2004;**3**(6):2299-2311

[25] Jalden J, Ottersten B. On the complexity of sphere decoding in digital communications. IEEE Transactions on Signal Processing. 2005;**53**(4): 1474-1484

[26] Burg A, Borgmann M, Wenk M, Zellweger M, Fichtner W, Bolcskei H. VLSI implementation of MIMO detection using the sphere decoding algorithm. IEEE Journal of Solid-State Circuits. 2005;**40**(7):1566-1577

[27] Hassibi B, Vikalo H. On the sphere-decoding algorithm. I. Expected complexity. IEEE Transactions on Signal Processing. 2005;**53**(8): 2806-2818

[28] Studer C, Burg A, Bolcskei H. Soft-output sphere decoding: Algorithms and VLSI implementation. IEEE Journal on Selected Areas in Communications. 2008;**26**(2):290-300

[29] Barbero LG, Thompson JS. Fixing the complexity of the sphere decoder for MIMO detection. IEEE Transactions on Wireless Communications. 2008;**7**(6): 2131-2142

[30] Nguyen TVH, Sugiura S, Lee K. Low-complexity sphere search-based adaptive spatial modulation. IEEE Transactions on Vehicular Technology. 2018;**67**(8):7836-7840

[31] Li L, Wen J, Tang X, Tellambura C. Modified sphere decoding for sparse code multiple access. IEEE Communications Letters. 2018;**22**(8): 1544-1547

[32] Karamanakos P, Geyer T, Aguilera RP. Long-horizon direct model predictive control: Modified sphere decoding for transient operation. IEEE Transactions on Industry Applications. 2018;**54**(6):6060-6070

[33] Tran TQ, Sugiura S, Lee K. Ordering- and partitioning-aided sphere decoding for generalized spatial

modulation. IEEE Transactions on Vehicular Technology. 2018;**67**(10): 10087-10091

[34] Vasudevan K, Madhu K, Singh S. Data detection in single user massive MIMO using re-transmissions. The Open Signal Processing Journal. 2019;**6**: 15-26. arXiv preprint arXiv:1811.11369. 2019. DOI: 10.2174/1876825301906010015

[35] Vasudevan K. Digital Communications and Signal Processing. 2nd ed. (CDROM included). Hyderabad: Universities Press (India); 2010. www.universitiespress.com

[36] Vasudevan K. Coherent detection of turbo coded OFDM signals transmitted through frequency selective Rayleigh fading channels. In: 2013 IEEE International Conference on Signal Processing, Computing and Control (ISPCC); 2013. pp. 1-6

[37] Vasudevan, K. Coherent detection of turbo-coded OFDM signals transmitted through frequency selective Rayleigh fading channels with receiver diversity and increased throughput. Wireless Personal Communications. 2015;**82**(3):1623-1642. DOI: 10.1007/s11277-015-2303-8

[38] Vasudevan K. Coherent detection of turbo-coded OFDM signals transmitted through frequency selective Rayleigh fading channels with receiver diversity and increased throughput. CoRR. Vol. abs/1511.00776; 2015. Available Online: http://arxiv.org/abs/1511.00776

[39] Vasudevan K. Coherent turbo coded MIMO OFDM. In: ICWMC 2016 - The 12th International Conference on Wireless and Mobile Communications; 2016. pp. 91-99

[40] Veludandi VK, Vasudevan K. Linear prediction-based detection of serially concatenated DQPSK in SIMO-OFDM. Wireless Personal Communications. 2017;**97**(3):4789-4811. DOI: 10.1007/s11277-017-4751-9

[41] Mishra HB, Vasudevan K. Design of superimposed training sequence for spatially correlated multiple-input multiple-output channels under interference-limited environments. IET Communications. 2015;**9**:1259-1268(9)

[42] Minn H, Bhargava VK, Letaief KB. A robust timing and frequency synchronization for OFDM systems. IEEE Transactions on Wireless Communications. 2003;**2**(4):822-839

[43] Tarokh V, Jafarkhani H. On the computation and reduction of the peak-to-average power ratio in multicarrier communications. IEEE Transactions on Communications. 2000;**48**(1):37-44

[44] Han SH, Lee JH. An overview of peak-to-average power ratio reduction techniques for multicarrier transmission. IEEE Wireless Communications. 2005;**12**(2):56-65

[45] Jiang T, Zhu G. Complement block coding for reduction in peak-to-average power ratio of OFDM signals. IEEE Communications Magazine. 2005;**43**(9): S17-S22

[46] Jiang T, Wu Y. An overview: Peak-to-average power ratio reduction techniques for OFDM signals. IEEE Transactions on Broadcasting. 2008; **54**(2):257-268

[47] Rahmatallah Y, Mohan S. Peak-to-average power ratio reduction in OFDM systems: A survey and taxonomy. IEEE Communication Surveys and Tutorials. 2013;**15**(4):1567-1592

[48] Wunder G, Fischer RFH, Boche H, Litsyn S, No J. The PAPR problem in OFDM transmission: New directions for

a long-lasting problem. IEEE Signal Processing Magazine. 2013;**30**(6): 130-144

[49] Sharma E, Mishra HB, Vasudevan K, Budhiraja R. PAPR analysis of superimposed training based SISO/MIMO-OFDM systems with orthogonal affine precoder. Physical Communication. 2017;**25**(P1):239-248. DOI: 10.1016/j.phycom.2017.08.004